Additional file 1

Development of the detection method for short-term slow slip events using GNSS data and its application to the Nankai subduction zone

Yutaro Okada, Takuya Nishimura, Takao Tabei, Takeshi Matsushima, Hitoshi Hirose

Corresponding author: okada.yutarou.24r@st.kyoto-u.ac.jp

Table. S1 List of the corrected postseismic deformation

		Fitting period 1*		Fitting period 2**	
Event name	Date (UT)	Start	End	Start	End
Tohoku-oki	Mar-11-2011	Jan-1-2006	Dec-31-2008	Jan-1-2011	Mar-10-2013
Off the Kii Peninsula	Sep-5-2004	Jan-1-2001	Dec-31-2002	Mar-5-2004	Dec-4-2004
Kumamoto	Apr-15-2016	Jan-1-2006	Dec-31-2008	Oct-15-2015	Jul-14-2016

*Period in which a secular velocity is estimated.

**Period in which a coseismic and postseismic displacement are estimated.

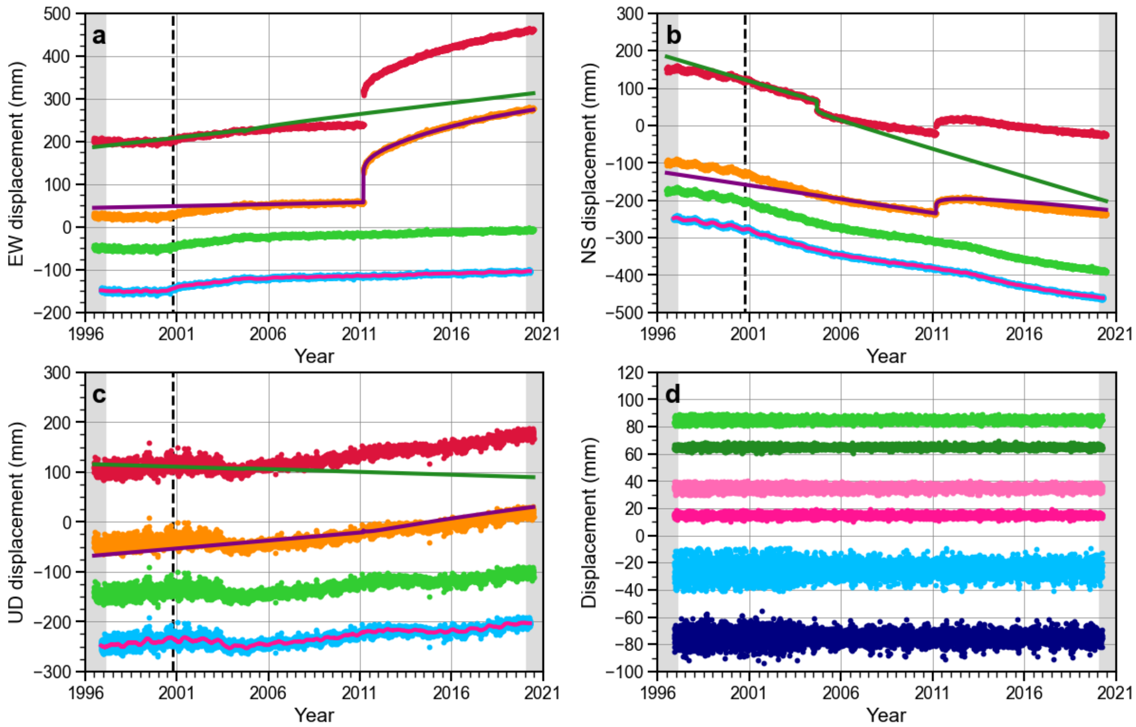

Fig. S1 GNSS time series at station 0301. **a** East-west (EW) component. Red dots represent the time series after correcting artificial offsets. The deep green line represents the estimated model of coseismic and postseismic deformation of the 2004 M_w 7.5 off the Kii Peninsula earthquake. Orange dots represent the corrected time series by using the deep green line. The purple line represents the estimated model of coseismic and postseismic deformation of the 2011 M_w 9.0 Tohoku-oki earthquake. Light green dots represent the corrected time series by using the purple line. The vertical black dashed line is the occurrence timing of the large earthquake. Sky-blue dots represent the time series after correcting the earthquake offset. A pink line represents a long-term trend. **b** Same as **a** but north-south (NS) component. **c** Same as **a** but up-down (UD) component. **d** Right green, right pink, and sky-blue dots represent the detrended time series of EW, NS, and UD component, respectively. Deep green, deep pink, and navy dots represent the EW, NS, and UD component time series after removing common-mode errors, respectively.

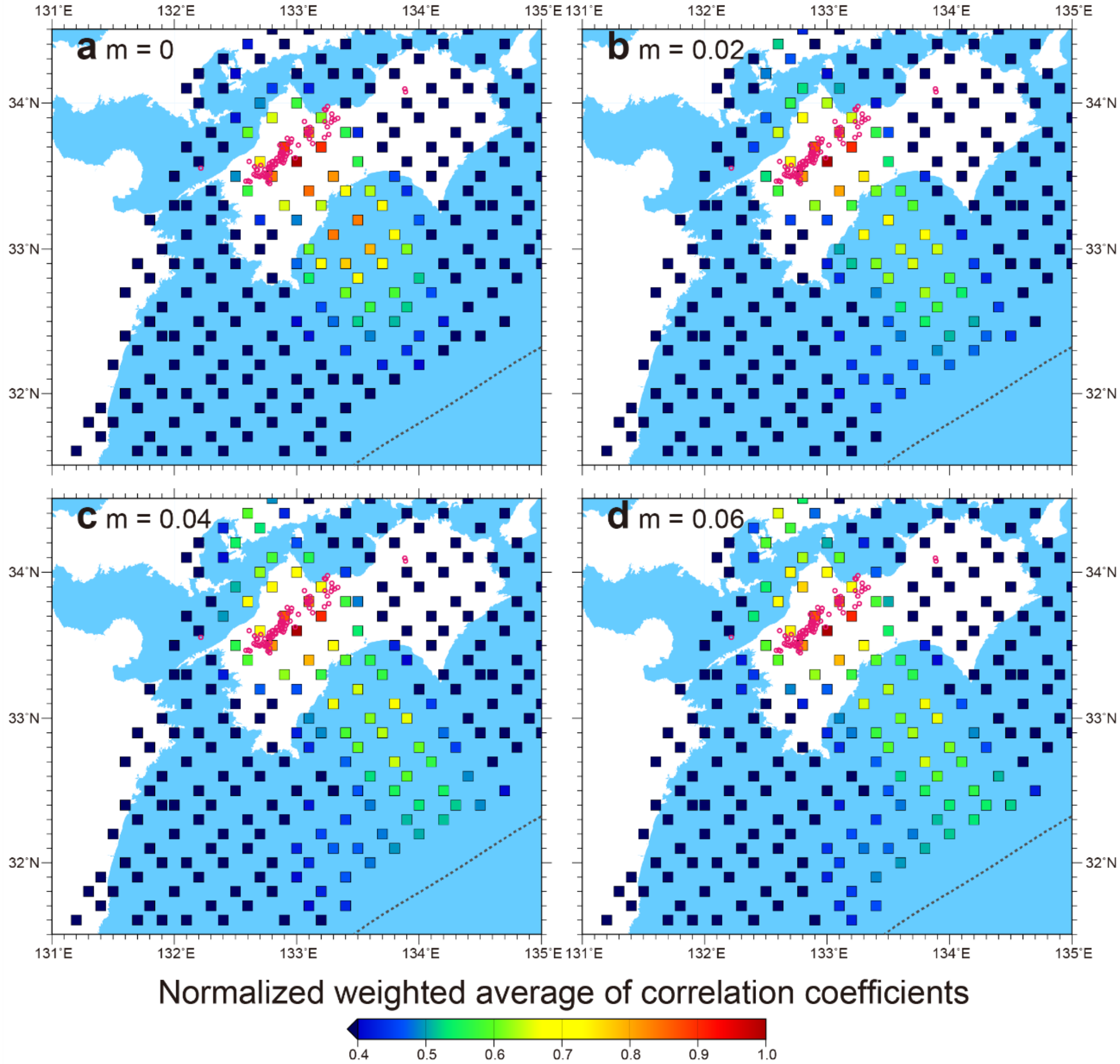

Fig. S2 Distribution of the normalized weighted average of correlation coefficients with different m values on April 18, 2005. We normalized the weighted averages by their maximum and minimum to show their spatial peak. Squares represent the center location of each sub-fault and their color shows the value of the normalized weighted average of correlation coefficients at the sub-fault. Pink circles represent the location of tremors. **a** $m = 0$. **b** $m = 0.02$. **c** $m = 0.04$. **d** $m = 0.06$.

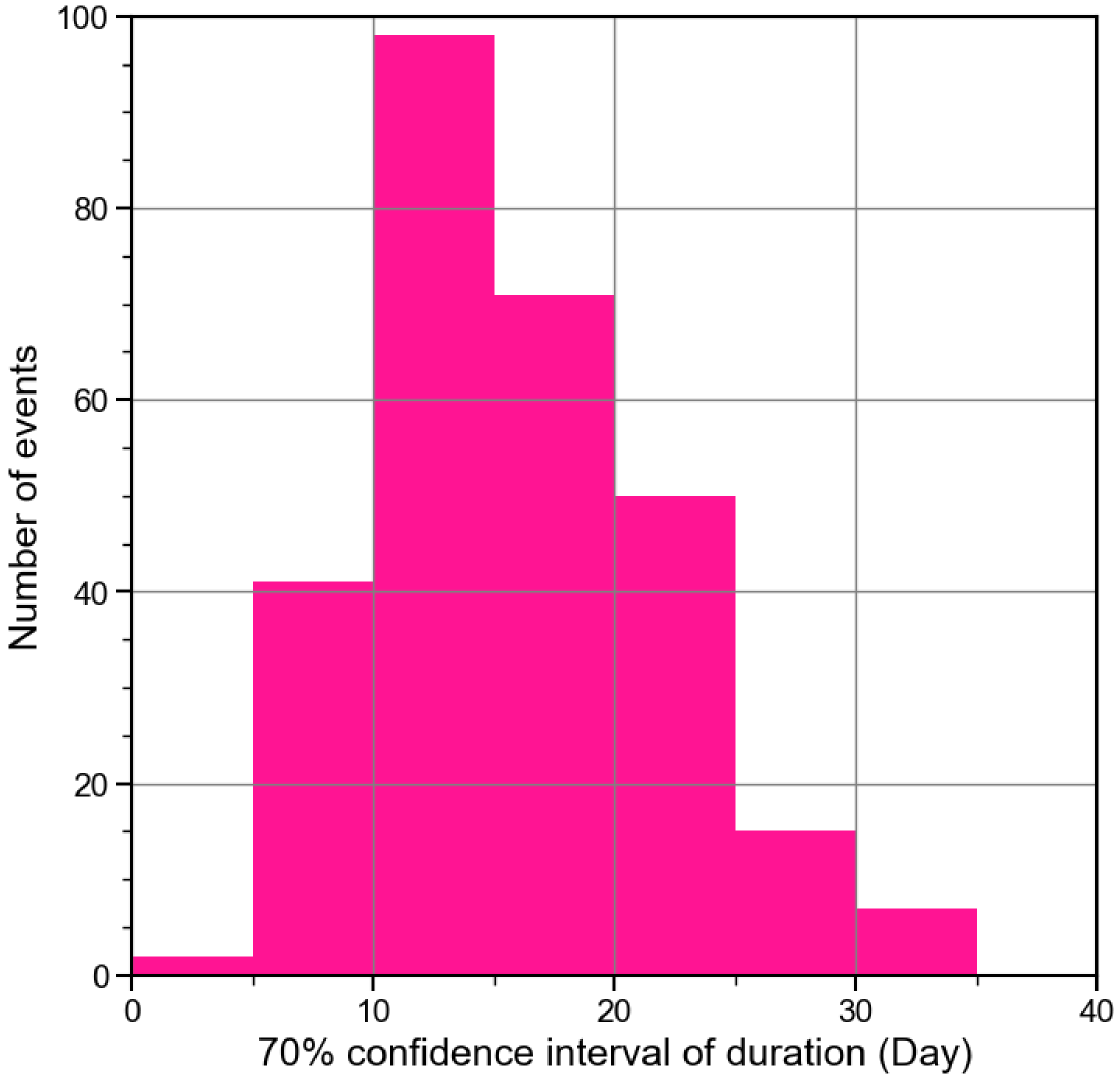

Fig. S3 Frequency distribution of the ranges of the 70% confidence interval of duration.

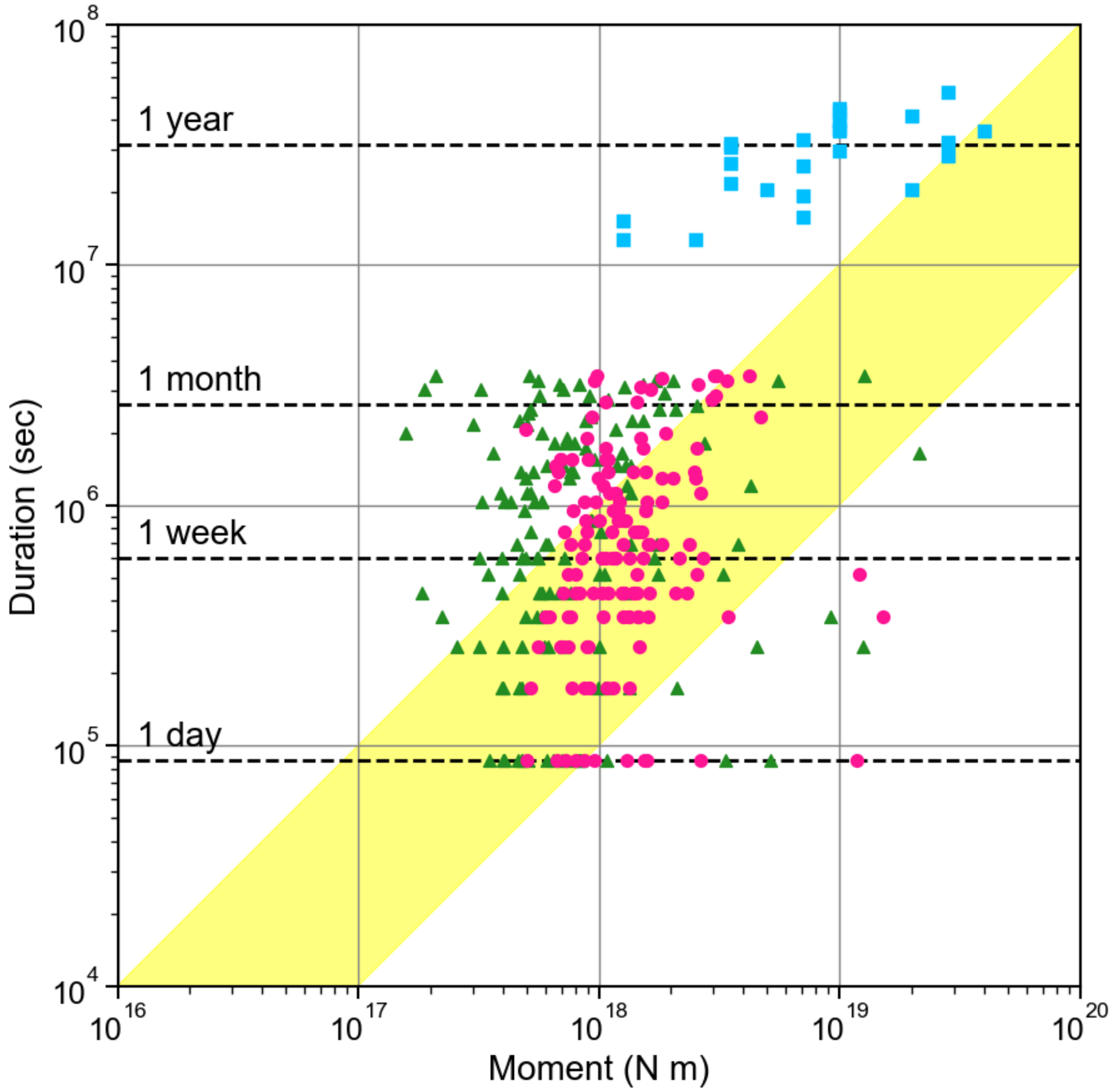

Fig. S4 Relationship between the moment and duration of SSEs in the Nankai subduction zone. Pink circles, green triangles, sky-blue squares, and the yellow shade represent class 1 SSEs, class 2 SSEs, L-SSEs (Takagi et al., 2019), and the scaling law between the moment and duration of slow earthquakes proposed by Ide et al. (2007), respectively.

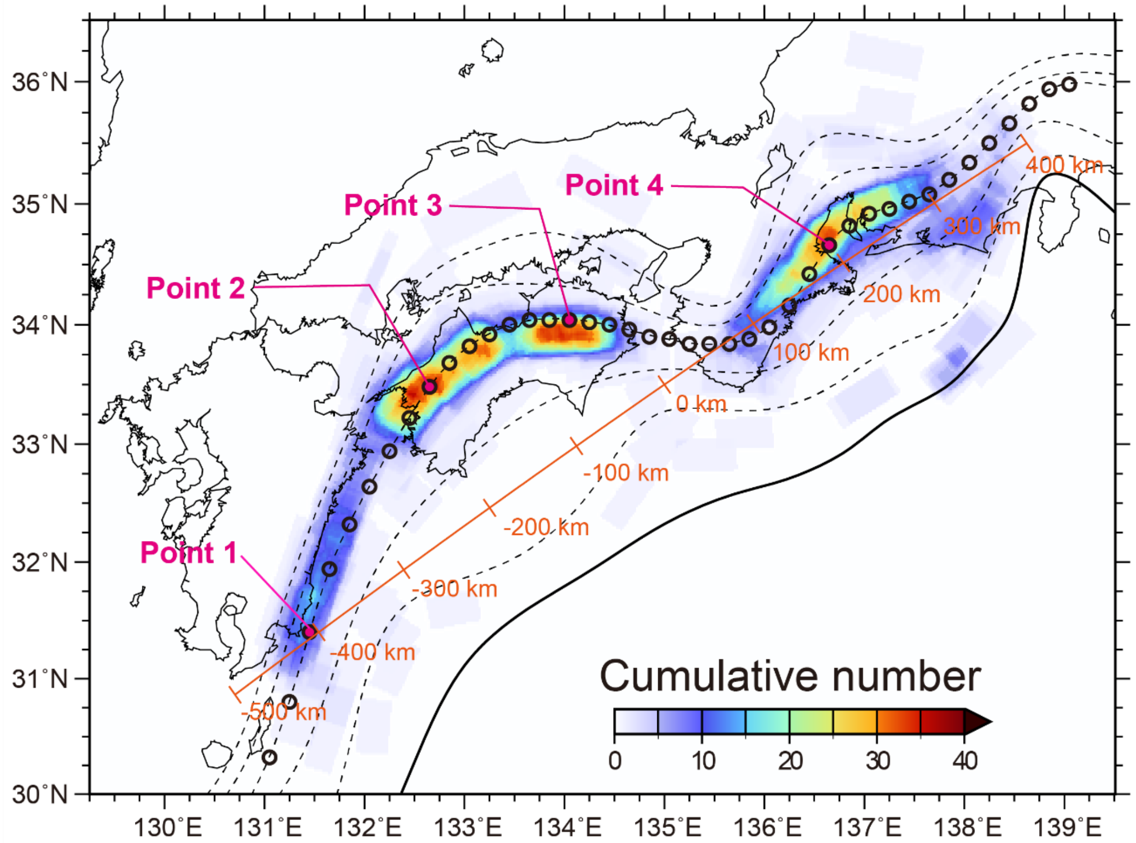

Fig. S5 Cumulative number of S-SSEs over 23 years. An orange line represents the distance used in Fig. S6. Black and pink dots represent calculation points aligned with the 30 km iso-depth contour (Iwasaki et al., 2015).

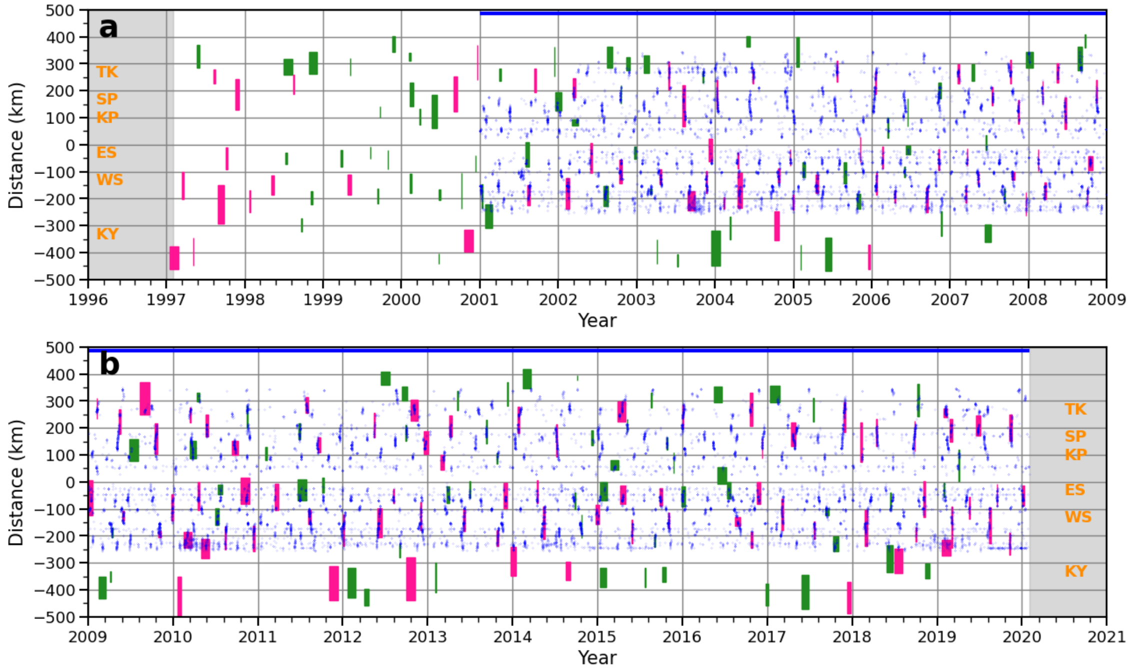

Fig. S6 Space-time plot of the detected S-SSEs. Pink and green rectangles represent the horizontal extent and duration of class 1 and class 2 SSEs at a depth of 10–50 km, respectively. Blue dots and line show tremors and the temporal extent of the tremor catalog (Maeda and Obara, 2009; Obara et al., 2010). KY, WS, ES, KP, SP, and TK represented by orange texts indicates the approximate location of Kyushu, western Shikoku, eastern Shikoku, the Kii Peninsula, the Shima Peninsula, and Tokai, respectively. The periods not applied to the detection are shaded in gray. **a** From 1996 to 2008. **b** From 2009 to 2020.

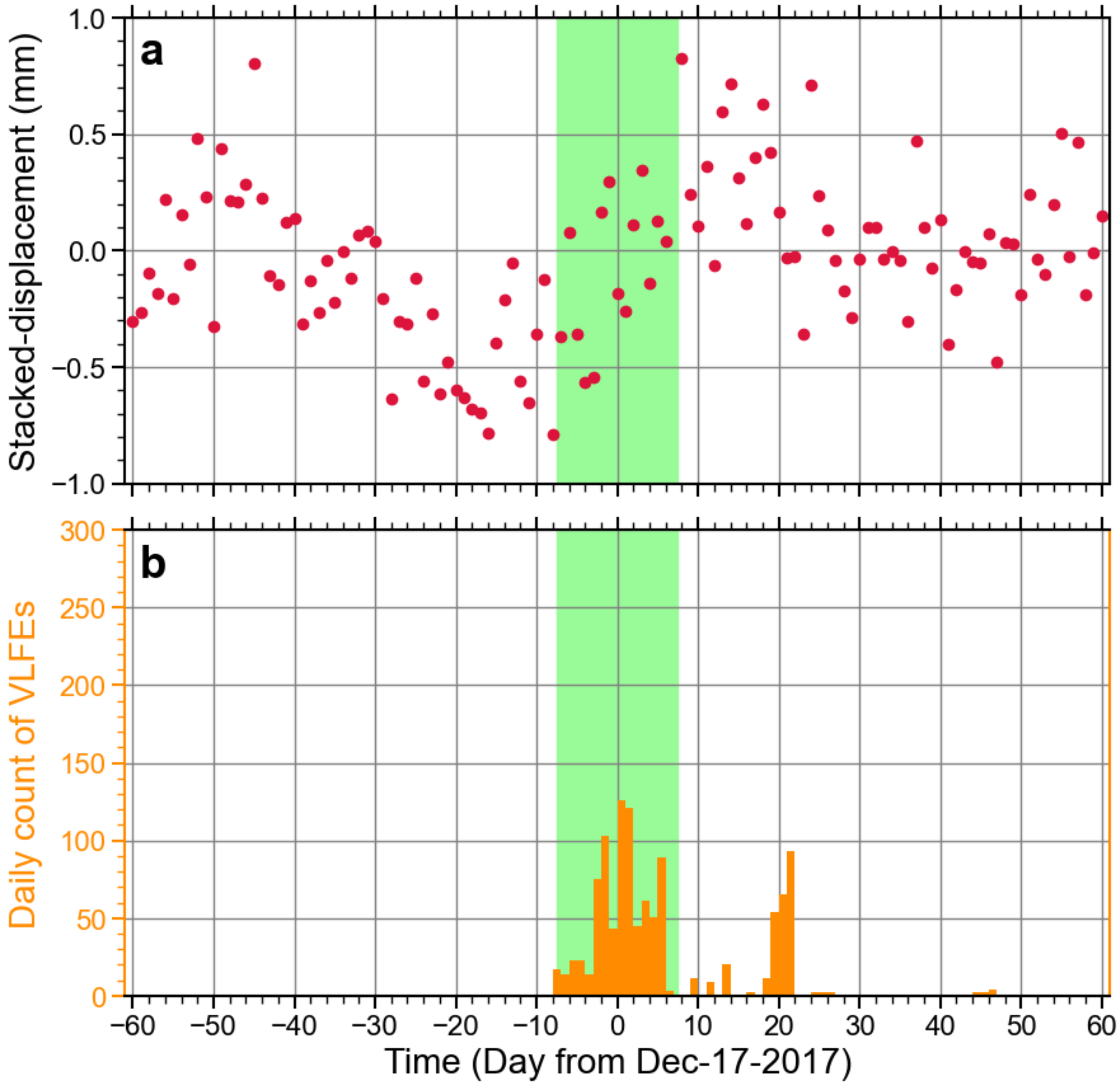

Fig. S7 Proximity of geodetic and seismic phenomena in the case of the December 2017 event (Additional file 1). **a** Stacked time series for the December 2017 S-SSE. Red dots and a green shaded area represent a stacked GNSS time series and the estimated duration of the S-SSE, respectively. **b** Activity of VLFEs (Baba et al., 2020) in the region of 130-133°E and 30-32.5°N. Yellow bars represent the daily count number of VLFEs.

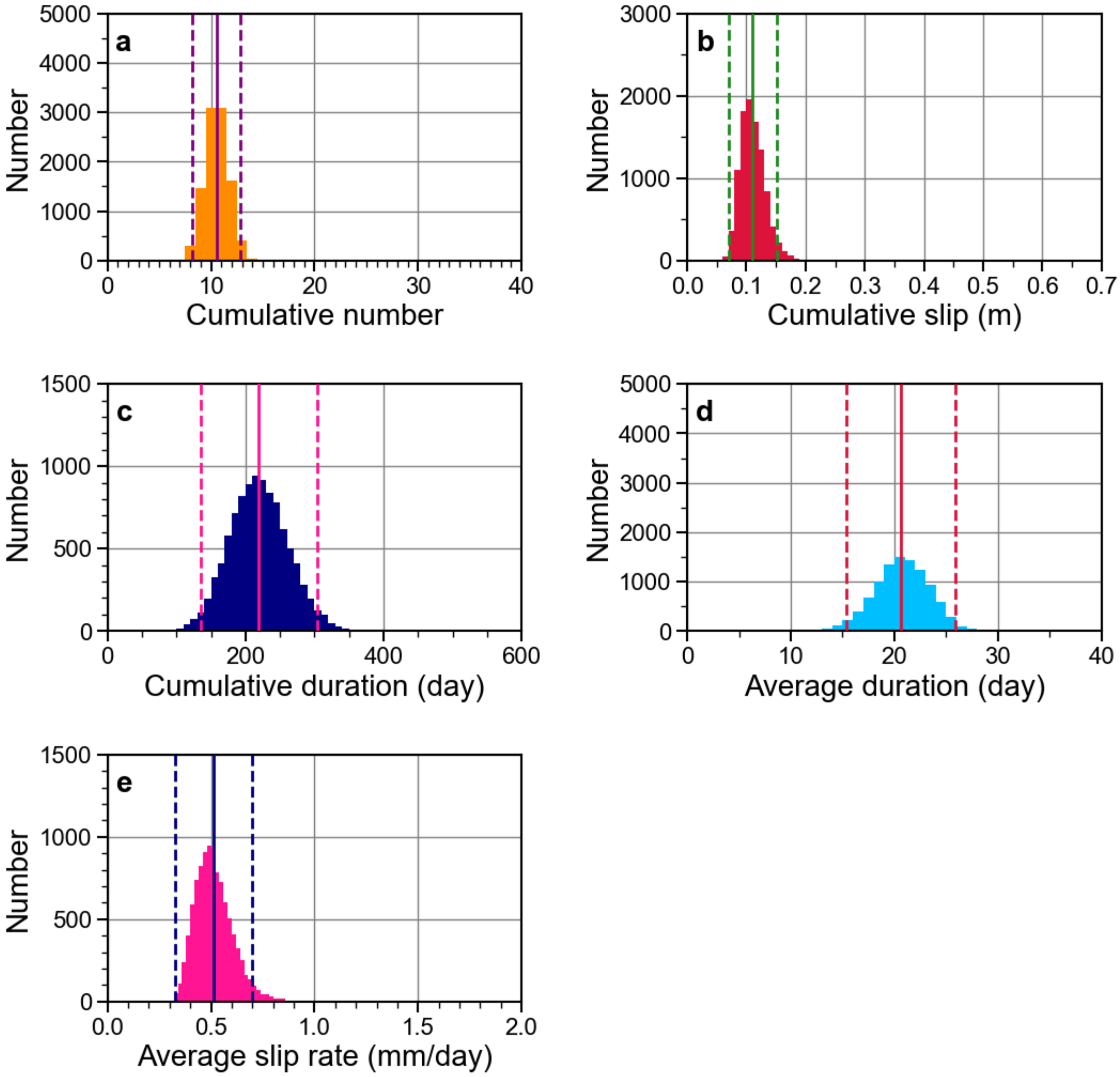

Fig. S8 **a** Frequency distribution of the cumulative number at Point 1. **b** Frequency distribution of the cumulative slip at Point 1. **c** Frequency distribution of the cumulative duration at Point 1. **d** Frequency distribution of the average duration at Point 1. **e** Frequency distribution of the average slip rate at Point 1. The purple, green, pink, and navy solid and dashed lines represent an average and 2-sigma interval, respectively.

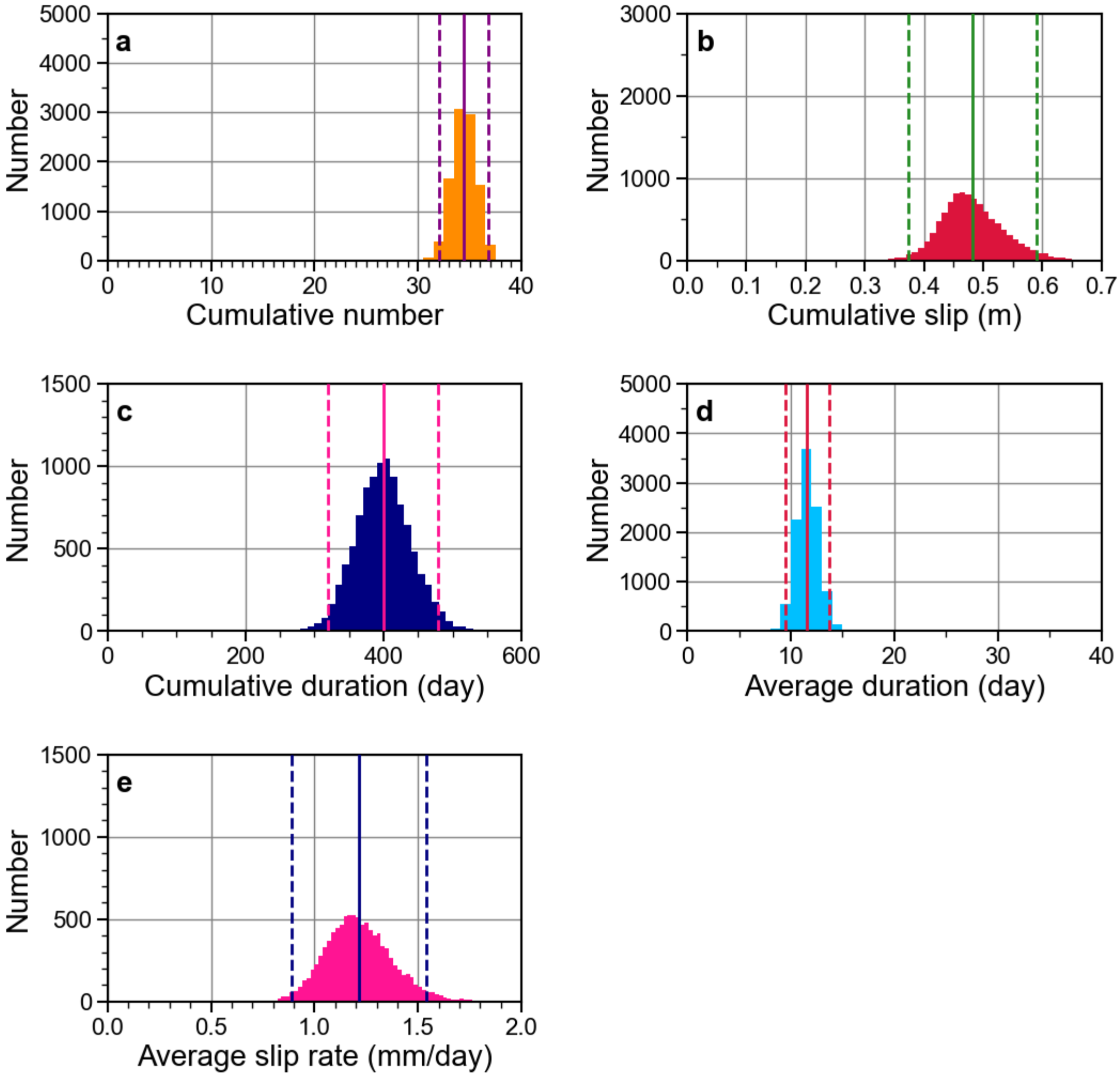

Fig. S9 Same as Fig. S8 but at Point 2.

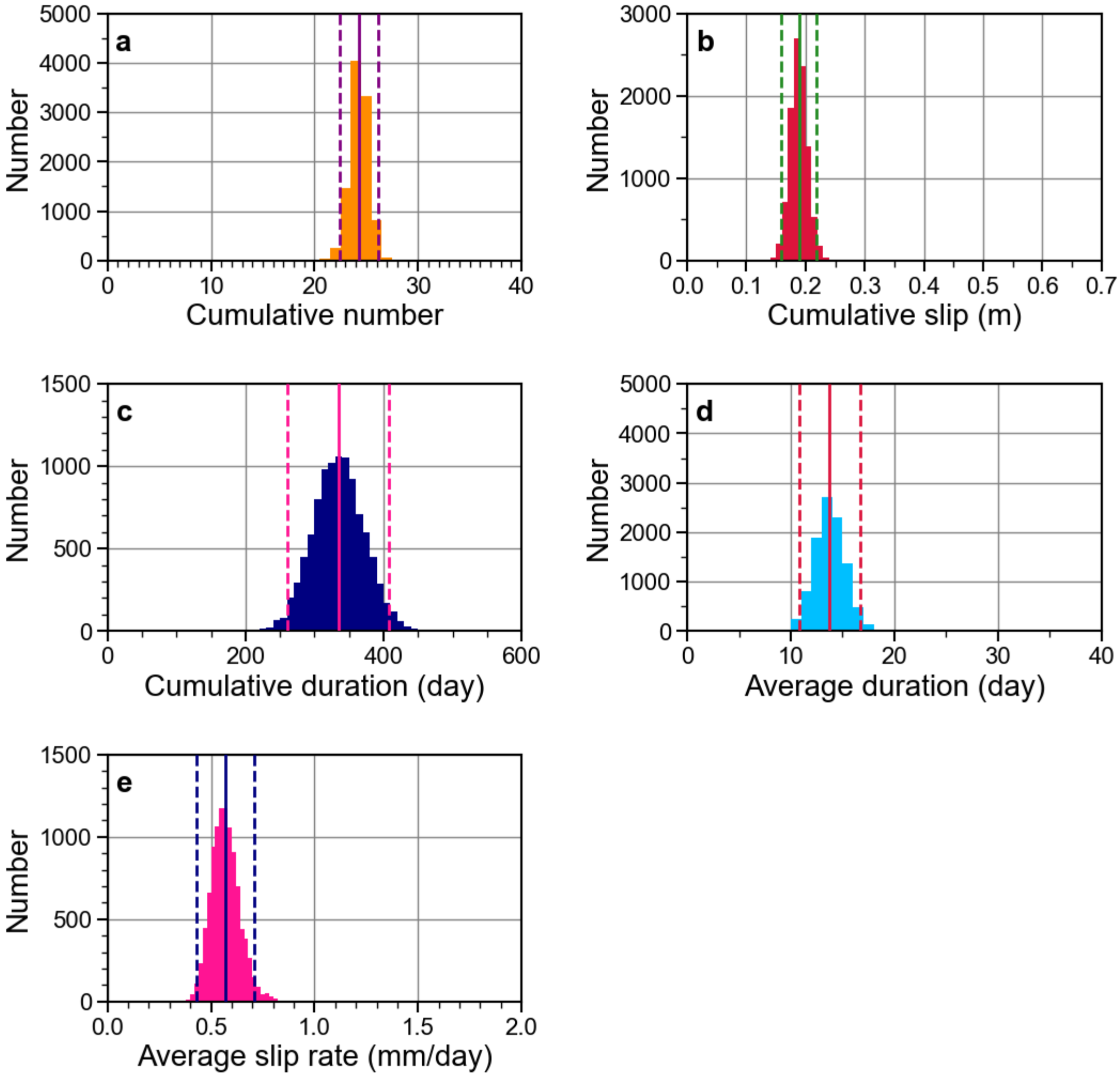

Fig. S10 Same as Fig. S8 but at Point 3.

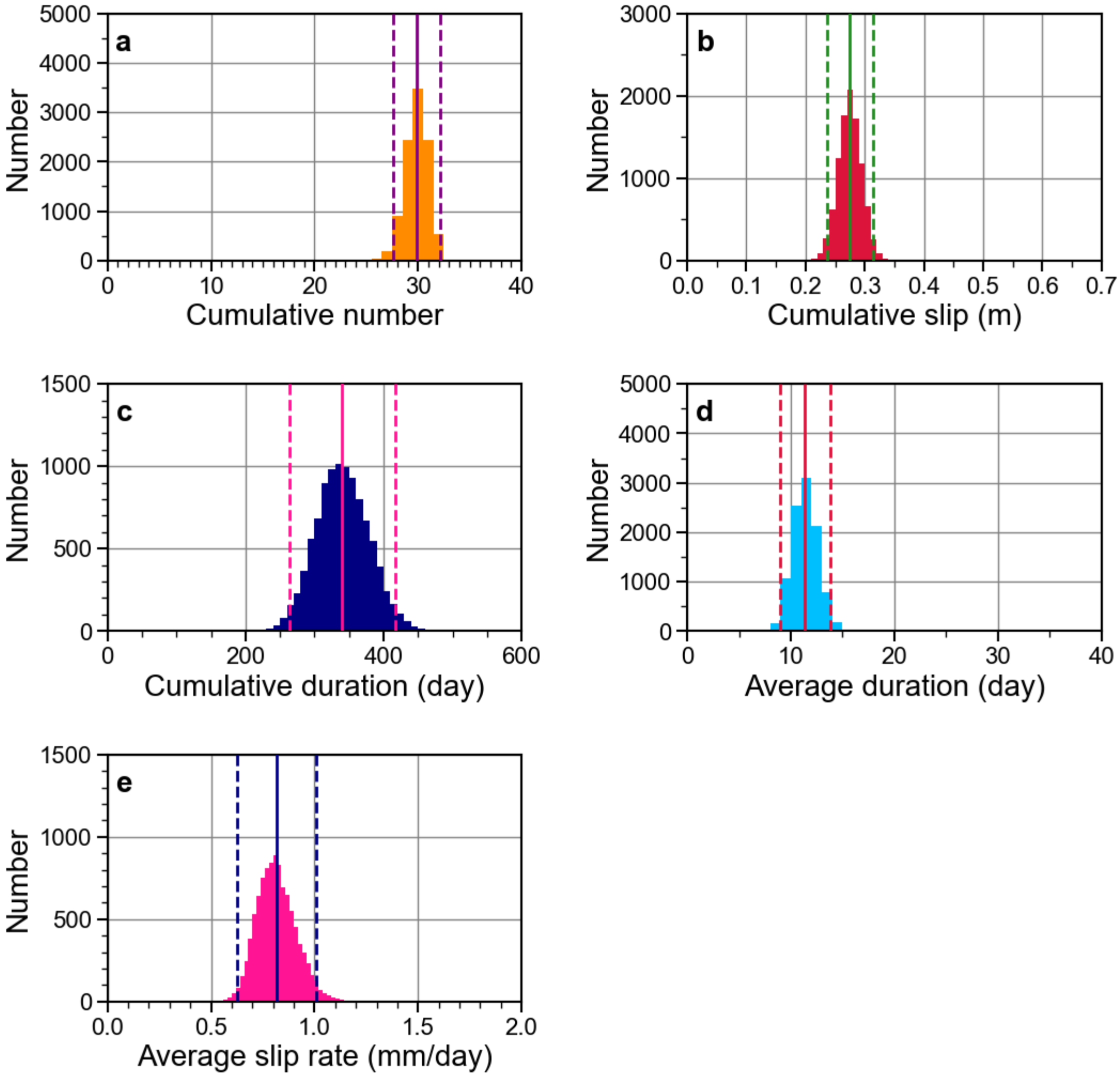

Fig. S11 Same as Fig. S8 but at Point 4.

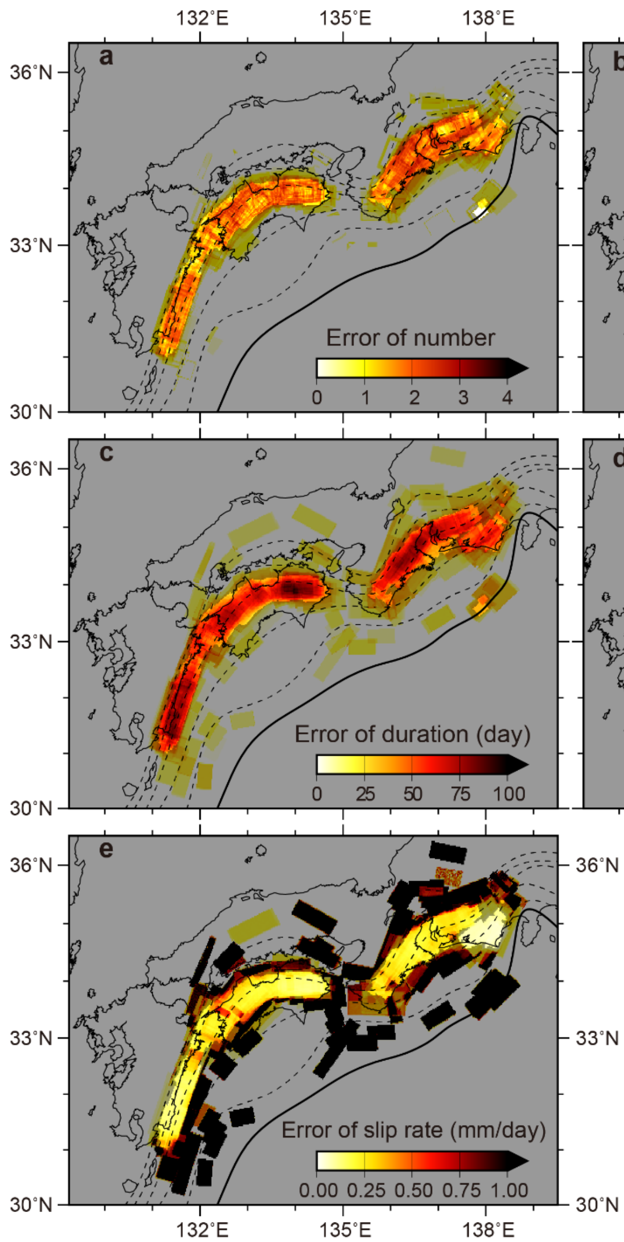

Fig. S12 **a** Error of cumulative number. **b** Error of cumulative slip. **c** Error of cumulative duration. **d** Error of average duration. **e** Error of average slip rate. The color represents twice the standard deviation of each value and the grid points experiencing less than five events on average are shaded.

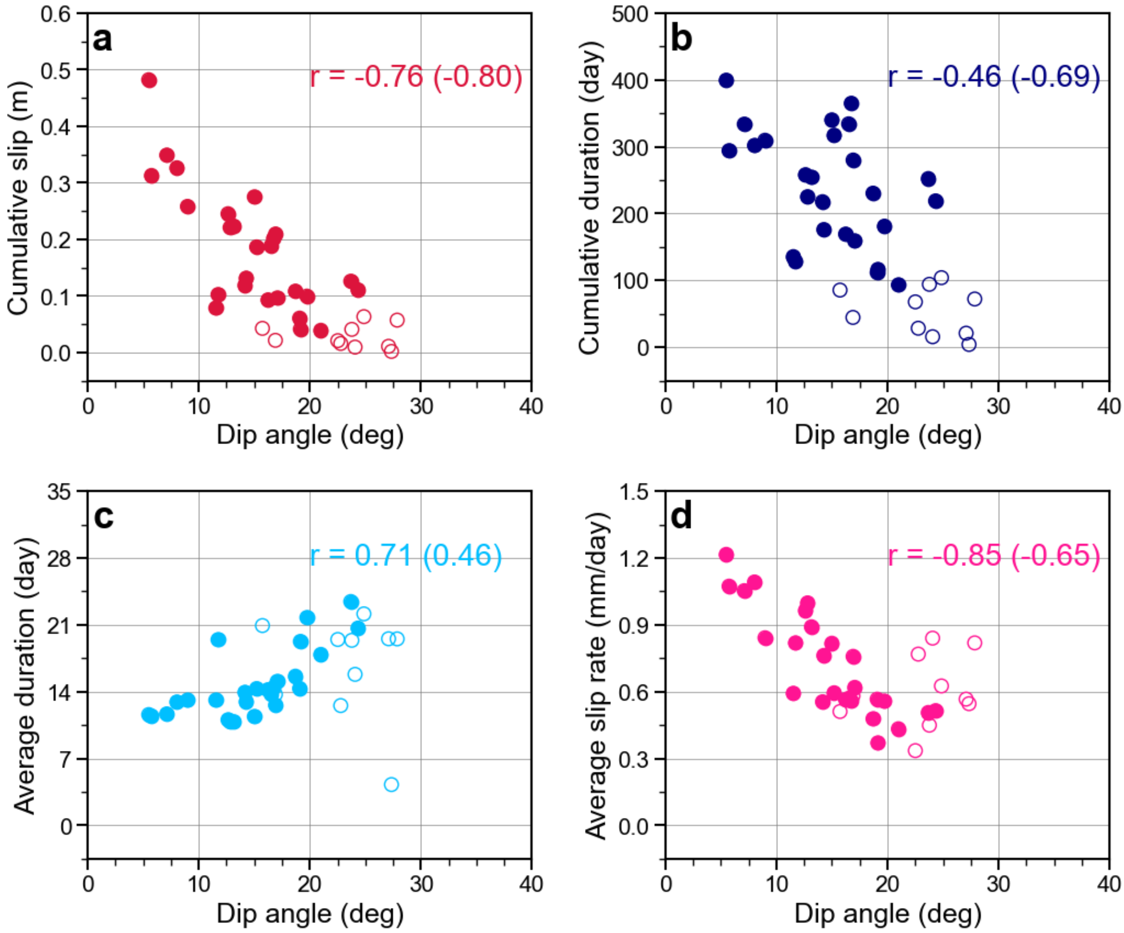

Fig. S13 a Relationship between the cumulative slip of S-SSEs and dip angles of the subducting plate (Iwasaki et al., 2015). They are calculated at the points along the 30 km iso-depth contour shown in Fig. S5. Note that the calculation points experiencing more than four events are plotted by solid symbols. A correlation coefficient between cumulative slip and dip angles is indicated with a character "r", and the values in and out of parenthesis represent the correlation coefficients calculated using all and solid symbols, respectively. **b** Same as **a** but the relationship between the cumulative duration and dip angles. **c** Same as **a** but the relationship between the average duration and dip angles. **d** Same as **a** but the relationship between the average slip rate and dip angles.

References

Baba S, Takemura S, Obara K, Noda A (2020) Slow earthquakes illuminating interplate coupling heterogeneities in subduction zones. Geophys Res Lett 47: e2020GL088089. doi:10.1029/2020GL088089

Ide S, Beroza GC, Shelly DR, Uchide T (2007) A scaling law for slow earthquakes. Nature 447:76-79. doi: 10.1038/nature0578076

Iwasaki T, Sato H, Shinohara M, Ishiyama T, Hashima A (2015) Fundamental structure model of island arcs and subducted plates in and around Japan. Paper presented at American Geophysical Union Fall Meeting 2015, San Francisco, December 14-18, 2015.

Maeda T, Obara K (2009) Spatiotemporal distribution of seismic energy radiation from low-frequency tremor in western Shikoku, Japan. J Geophys Res 114:B00A09. doi:10.1029/2008JB006043

Obara K, Tanaka S, Maeda T, Matsuzawa T (2010) Depth-dependent activity of non-volcanic tremor in southwest Japan. Geophys Res Lett 37:L13306. doi:10.1029/2010GL043679

Takagi R, Uchida N, Obara K (2019) Along-strike variation and migration of long-term slow slip events in the western Nankai subduction zone, Japan. J Geophys Res Solid Earth 124:3853-3880. doi:10.1029/2018JB016738